

THE NEUTRAL GAS DYNAMICS OF THE NEARBY MAGELLANIC IRREGULAR GALAXY UGCA 105

JOHN M. CANNON¹, ELIJAH Z. BERNSTEIN-COOPER¹, IAN M. CAVE¹, JON B. HARRIS¹, MELISSA V. MARSHALL¹, JACOB M. MOEN¹, SAMILEE J. MOODY¹, ERIN M. O'LEARY¹, STEPHEN A. PARDY¹, CLARA M. THOMANN¹

The Astronomical Journal, in press

ABSTRACT

We present new low-resolution HI spectral line imaging, obtained with the *Karl G. Jansky Very Large Array (JVLA)*, of the star-forming Magellanic irregular galaxy UGCA 105. This nearby ($D = 3.39 \pm 0.25$ Mpc), low mass ($M_{\text{HI}} = 4.3 \pm 0.5 \times 10^8 M_{\odot}$) system harbors a large neutral gas disk (HI radius ~ 7.2 kpc at the $N_{\text{HI}} = 10^{20} \text{ cm}^{-2}$ level) that is roughly twice as large as the stellar disk at the B-band R_{25} isophote. We explore the neutral gas dynamics of this system, fitting tilted ring models in order to extract a well-sampled rotation curve. The rotation velocity rises in the inner disk, flattens at $72 \pm 3 \text{ km s}^{-1}$, and remains flat to the last measured point of the disk (~ 7.5 kpc). The dynamical mass of UGCA 105 at this outermost point, $(9 \pm 2) \times 10^9 M_{\odot}$, is ~ 10 times as large as the luminous baryonic components (neutral atomic gas and stars). The proximity and favorable inclination (55°) of UGCA 105 make it a promising target for high resolution studies of both star formation and rotational dynamics in a nearby low-mass galaxy.

Subject headings: galaxies: evolution — galaxies: dwarf — galaxies: irregular — galaxies: individual (UGCA 105)

1. INTRODUCTION

Dwarf galaxies offer an opportunity to study various processes that bear on galaxy evolution. Nearby systems allow an exploration of the interplay between ongoing star formation and the multi-phase interstellar medium (ISM). Further, nearby gas-rich systems are amenable to detailed studies of galactic rotational dynamics in the absence of differential shear. Many dwarfs display solid-body rotation that is well-suited to precision rotation curve work (e.g., Oh et al. 2008). Most nearby systems appear to be dark-matter dominated (Mateo 1998), making them important laboratories for studying both the luminous and the dark mass components in galaxies.

UGCA 105 (see Table 1 for representative qualities) is a Magellanic-type irregular galaxy with ongoing star formation [recent star formation as traced by the H α emission line has been studied by Kennicutt et al. (2008), Lee et al. (2009), and Karachentsev & Kaisin (2010); while the total H α luminosities differ slightly between these works, each finds a significant H α -based ongoing star formation rate of $\sim 0.06\text{--}0.07 M_{\odot} \text{ yr}^{-1}$]. Its relative proximity makes it well-suited for detailed studies of the ISM. Using the magnitudes of the brightest stars, Tikhonov et al. (1992) and Karachentsev et al. (1997) estimated distances of 3.2–3.3 Mpc. Subsequent observations with the *Hubble Space Telescope (HST)* provided a distance based on the magnitude of the tip of the red giant branch (TRGB; $M_I = -4.05 \pm 0.02$, with little dependence on metallicity; see Rizzi et al. 2007 and references therein) of 3.15 ± 0.32 Mpc (Karachentsev et al. 2002). Subsequent analyses by Jacobs et al. (2009) and by the authors of the Extragalactic Distance Database (Tully et al. 2009; B. Jacobs, private communication) revise this slightly upward to 3.39 ± 0.25 Mpc. We adopt this distance measurement throughout the present work. At 3.39 Mpc, $1''$ corresponds to 16.4 pc.

As Figure 1 shows, the stellar disk has an irregular morphology and harbors numerous high surface brightness HII regions and widespread diffuse H α emission. Despite these characteristics, UGCA 105 has by comparison remained poorly studied in the literature. The low Galactic latitude of the system (13.7°) and the significant foreground extinction values ($E(B-V) = 0.351$ mag, or 1.51 mag of extinction in the B-band; see discussion in footnotes to Table 1) may have conspired to keep this system out of many mainstream local galaxy surveys. As we show in this work, the stellar and gaseous components of UGCA 105 contain rich morphological and kinematic structure. This work presents the first detailed study of the neutral gas dynamics of this nearby dwarf galaxy.

2. OBSERVATIONS AND DATA HANDLING

HI spectral line imaging of UGCA 105 was obtained with the National Radio Astronomy Observatory's *Karl G. Jansky Very Large Array (JVLA)*² on October 10, 2011. These data were acquired under the auspices of the “Observing for University Classes” program for an upper-level astronomical techniques class at Macalester College. The program was officially classified as a “Demonstration Science” program and carries the legacy program identification of TDEM0015.

The observations were acquired during a two-hour observation block with the observatory in the D (most compact) configuration. The WIDAR correlator was used in a standard Open Shared Risk Observing single polarization mode, providing 128 channels over a 2 MHz wide bandwidth. The resulting channel separation of $15.625 \text{ kHz ch}^{-1}$ corresponds to $3.3 \text{ km s}^{-1} \text{ ch}^{-1}$ at the rest frequency of the HI spectral line. Reductions followed standard prescriptions and used both the Astronomical Image Processing System (AIPS) and the Common Astronomy Software Applications (CASA) packages.

¹ Department of Physics & Astronomy, Macalester College, 1600 Grand Avenue, Saint Paul, MN 55105; jcannon@macalester.edu

² The National Radio Astronomy Observatory is a facility of the National Science Foundation operated under cooperative agreement by Associated Universities, Inc.

TABLE 1
BASIC CHARACTERISTICS OF UGCA 105

Parameter	Value
Right ascension (J2000)	05 ^h 14 ^m 15. ^{s3}
Declination (J2000)	+62°34'48"
Adopted distance (Mpc)	3.39 ^a
E(B−V) (Mag.)	0.351 ^b
M _B (Mag.)	−14.70 ^c
Interferometric S _{HI} (Jy km s ^{−1})	159.9 ± 16
Single-dish S _{HI} (Jy km s ^{−1})	163.45 ^d
HI mass M _{HI} (M _⊙)	(4.3 ± 0.5) × 10 ⁸
HI major axis diameter (kpc)	~14.4 ^e
B-band R ₂₅ (kpc)	7.5 ^f

^aJacobs et al. (2009); Tully et al. (2009)

^bFrom the Extragalactic Distance Database (Jacobs et al. 2009, Tully et al. 2009). Note that Schlegel et al. 1998 find E(B−V)=0.313, but that this value is revised upward based on the properties of resolved stars (B. Jacobs, private communication).

^cCalculated using the observed m_B=14.46 ± 0.22 from Kennicutt et al. (2008), the distance value from this table, and assuming that the foreground Galactic reddening produces A_B=1.51 magnitudes of extinction.

^dSpringob et al. (2005); note that those authors apply a ~24% correction for pointing and HI self-absorption, raising the flux integral to 203.34 ± 21.07 Jy km s^{−1}.

^eMeasured as the major axis diameter at the N_{HI} = 10²⁰ cm^{−2} level.

^fMeasured as the B-band major axis diameter at the 25.0 mag arcsec^{−2} isophote from de Vaucouleurs et al. (1991).

UGCA 105 has a low systemic velocity ($V_{\text{sys}} = 90.8 \pm 2.0 \text{ km s}^{-1}$, derived from the tilted ring analysis discussed in § 3.2) for its distance well outside the Local Group, and hence HI emission from UGCA 105 is relatively close in velocity space to the foreground emission from the Milky Way. The selection of the band center frequency and the 2 MHz bandwidth was adequate to cleanly separate the Milky Way and UGCA 105 emission components. Roughly 40 line-free channels were available at velocities higher than those occupied by the target galaxy, and these were used to fit the underlying continuum with a first-order polynomial and remove it from all channels of the cube. UGCA 105 occupies roughly 54 channels of the cube; Milky Way contamination is severe in the ~25 lowest-velocity channels, and about 8 channels separate UGCA 105 and the foreground components. To be cautious, we do not use these 8 line-free channels in the continuum removal. We conclude that foreground Milky Way emission does not affect the portions of our cubes that contain HI spectral line emission from UGCA 105.

The final spectral line cube used in this analysis was produced using the AIPS IMAGR task with a ROBUST weighting of 0.5; this cube was cleaned to the rms level (0.003 Jy beam^{−1}) found in 2-3 line-free channels (purposefully included in the cube and not including emission from UGCA 105). This original cube has a resolution element of 53.58" × 42.01". To produce the moment maps used below, we follow procedures similar to those described in Cannon et al. (2009, 2010, 2011). The full-resolution spectral line cube is convolved to a circular

beam size of 60". The rms noise level in the line-free channels of this convolved cube is found to be 0.0025 Jy beam^{−1}. The convolved cube is blanked at 2.5 times this rms level (0.00625 Jy beam^{−1}), and the resulting blanked cube is then carefully examined by hand to identify regions of “real” emission that are present in three or more consecutive channels. This blanked cube is then used as a template to blank the original cube when convolved to the smallest possible circular beam size. Thus, the final data cube produced here has a 54" circular beam (physical resolution element = 890 pc). The noise in the final cube is 0.0047 Jy beam^{−1}.

The first two moment maps at 54" resolution (representing integrated intensity and intensity weighted velocity) were created from this data cube using the XMOM task in AIPS. The final moment zero image was converted to column density units (atoms cm^{−2}) using standard relations. Edge effects in the final moment maps were minimized by blanking the final moment zero image below the 1 × 10²⁰ cm^{−2} level, and using this same level for all moment maps. The images of integrated HI emission are discussed in detail in § 3.

The total HI flux integral, derived from the 54" cube, is 159.9 ± 16 Jy km s^{−1}; this is in excellent agreement with the single-dish flux integral of 163.45 Jy km s^{−1} found by Springob et al. (2005; however, those authors do apply an upward ~24% correction for HI self-absorption, bringing their absorption-corrected flux integral to 203.34 ± 21.07 Jy km s^{−1}). Using the flux integral derived from our *JVLA* imaging, we derive a total HI mass of (4.3 ± 0.5) × 10⁸ M_⊙.

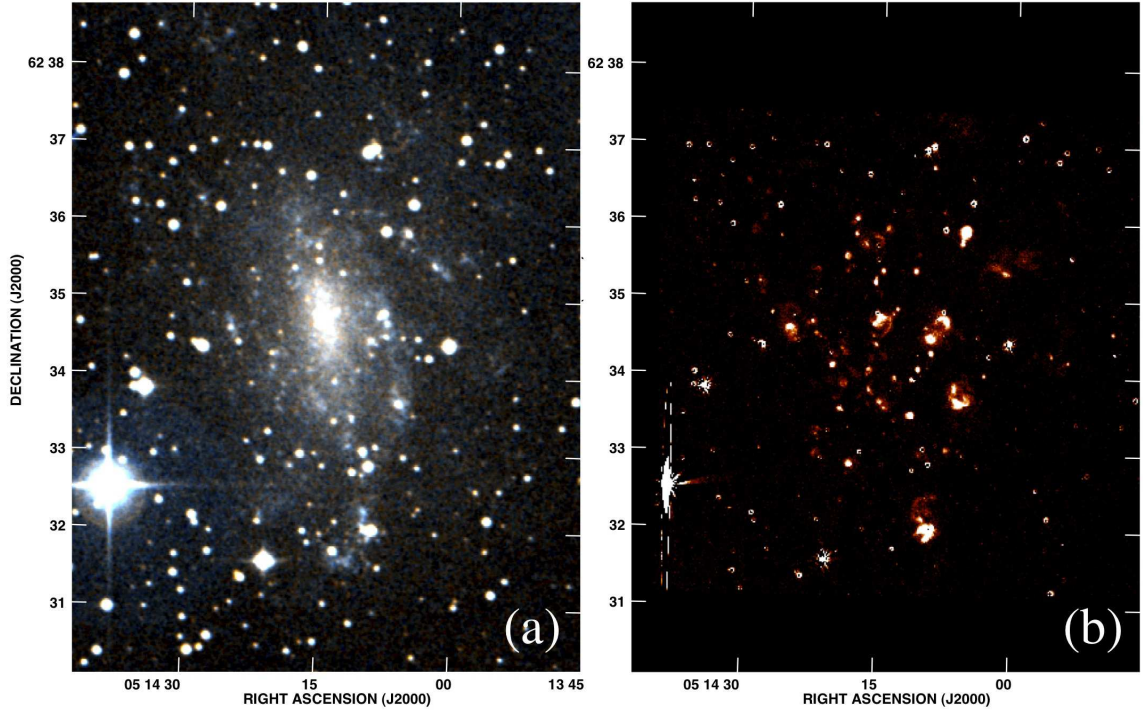


FIG. 1.— (a) 3-color image of UGCA 105 created from B, V, and R band *Digitized Sky Survey* images. The faint arc of blue emission in the upper right corner is scattered light from a bright foreground star off the field of view. (b) Continuum-subtracted $H\alpha$ image of UGCA 105 (image courtesy Janice Lee and Robert C. Kennicutt, Jr.). There are multiple star formation regions throughout the disk of UGCA 105. The field of view shown in these images is smaller than that shown in Figure 6.

During the reduction of the HI spectral line data, we averaged 28 line-free channels to produce a 1.4 GHz radio continuum image. This image has a beam size of $53.6'' \times 41.6''$ and an rms noise level of 6.5×10^{-4} Jy beam $^{-1}$. There is weak positive point source emission detected in the southern part of the disk of UGCA 105. This source is catalogued in NVSS images (Condon et al. 1998) as NVSS J051418+623136 with a flux density of 2.1×10^{-2} Jy; we measure a flux density of $(1.6 \pm 0.5) \times 10^{-2}$ Jy in our continuum image. This object is most likely a background continuum source, such as a QSO, and is not coincident with any high surface brightness $H\alpha$ emission from UGCA 105 (see Figure 1). The 5σ upper limit to the global 1.4 GHz radio continuum flux density from UGCA 105 is derived to be $S_{1.4\text{GHz}} \lesssim 3.2 \times 10^{-3}$ Jy. This flux density is comparable to the total thermal radio continuum flux expected based on the strength of the integrated $H\alpha$ emission (Kennicutt et al. 2008 publish a total $H\alpha + [\text{N II}]$ flux of 2.5×10^{-12} erg s $^{-1}$ cm $^{-2}$) using the prescriptions in Caplan & Deharveng (1986). Given these limitations, and the distributed star formation throughout the disk of UGCA 105 (see Figure 1), we do not study the detailed nature of the radio continuum emission in UGCA 105 with the present data.

3. GASEOUS, STELLAR, AND DARK COMPONENTS

3.1. The Neutral Gas Distribution and Dynamics

HI emission from UGCA 105 is detected at high significance in 54 channels spanning the heliocentric radial velocity range of $168.1 - -6.6$ km s $^{-1}$. Figures 2 and 3 show the individual channel maps of the $54''$ -resolution datacube. The ordered rotation of the system is prominent as a classical “butterfly diagram” moving from southwest

to northeast with increasing heliocentric velocity. The HI surface brightness is slightly lower in the southwest region of the disk compared to the northeast, although the bulk kinematics are very well defined throughout the disk.

We create the global HI profile shown in Figure 4 by summing the flux in each of the channel maps shown in Figures 2 and 3. As expected from the “butterfly diagram” noted above, we see a classic double-horn HI line profile. The higher velocity (northeast) region of the disk shows a slightly higher integrated flux per channel. We fit this profile to derive the systemic velocity of the system (95 ± 5 km s $^{-1}$). We refine this estimate in our kinematic analysis (see below) to $V_{\text{sys}} = 90.8 \pm 2$ km s $^{-1}$, and show V_{sys} as a vertical line in Figure 4.

Figure 5 shows two-dimensional images of the HI morphology and kinematics. The moment 0 (integrated HI intensity) images show rich morphological structure in the neutral gas disk. There is low surface brightness HI gas in the outer disk, but throughout most of the inner disk the column densities rise above 10^{21} cm $^{-2}$ at $54''$ (890 pc) resolution. There are regions of the inner disk with comparatively low HI column densities that are roughly the size of the synthesized beam. While these features are suggestive of HI holes and shells, we await higher spatial resolution imaging in order to study these features in detail.

As expected from the well-behaved channel maps shown in Figures 2 and 3, the intensity weighted velocity field shown in Figure 5 is very symmetric at this physical resolution. Within the inner disk the isovelocity contours are mostly parallel and the major axis of rotation is well-defined (position angle $\sim 15^\circ$ east of north; see more detailed discussion below). The bulk gas kinemat-

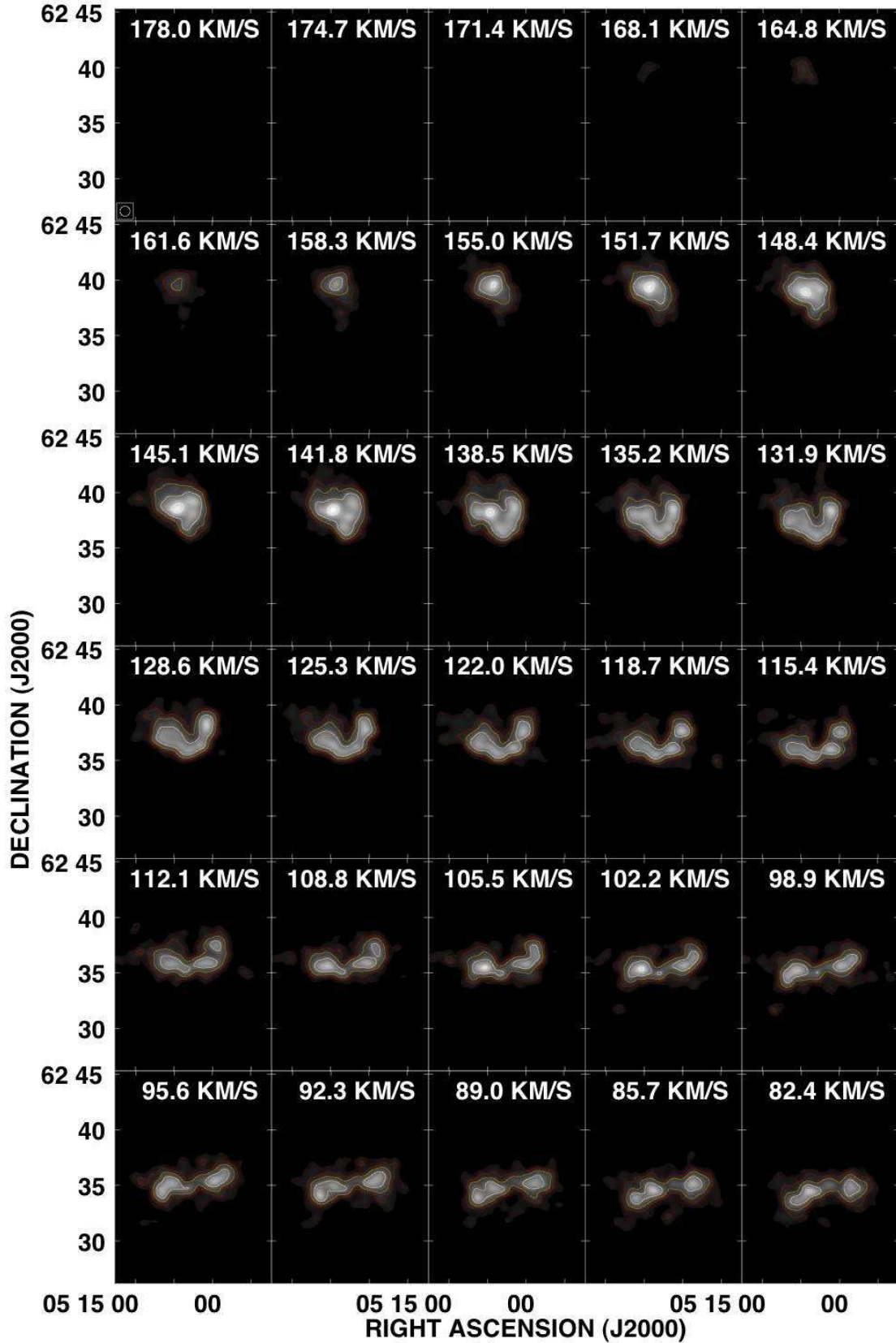


FIG. 2.— 30 channel maps from the $54''$ resolution datacube; heliocentric velocity is noted in each frame, and the beam size is shown in the top left panel. Contours are at levels of (3,6,12,24,48) σ , where $\sigma=2.5 \times 10^{-3}$ Jy beam $^{-1}$ is the rms noise measured in line-free channels of the cube.

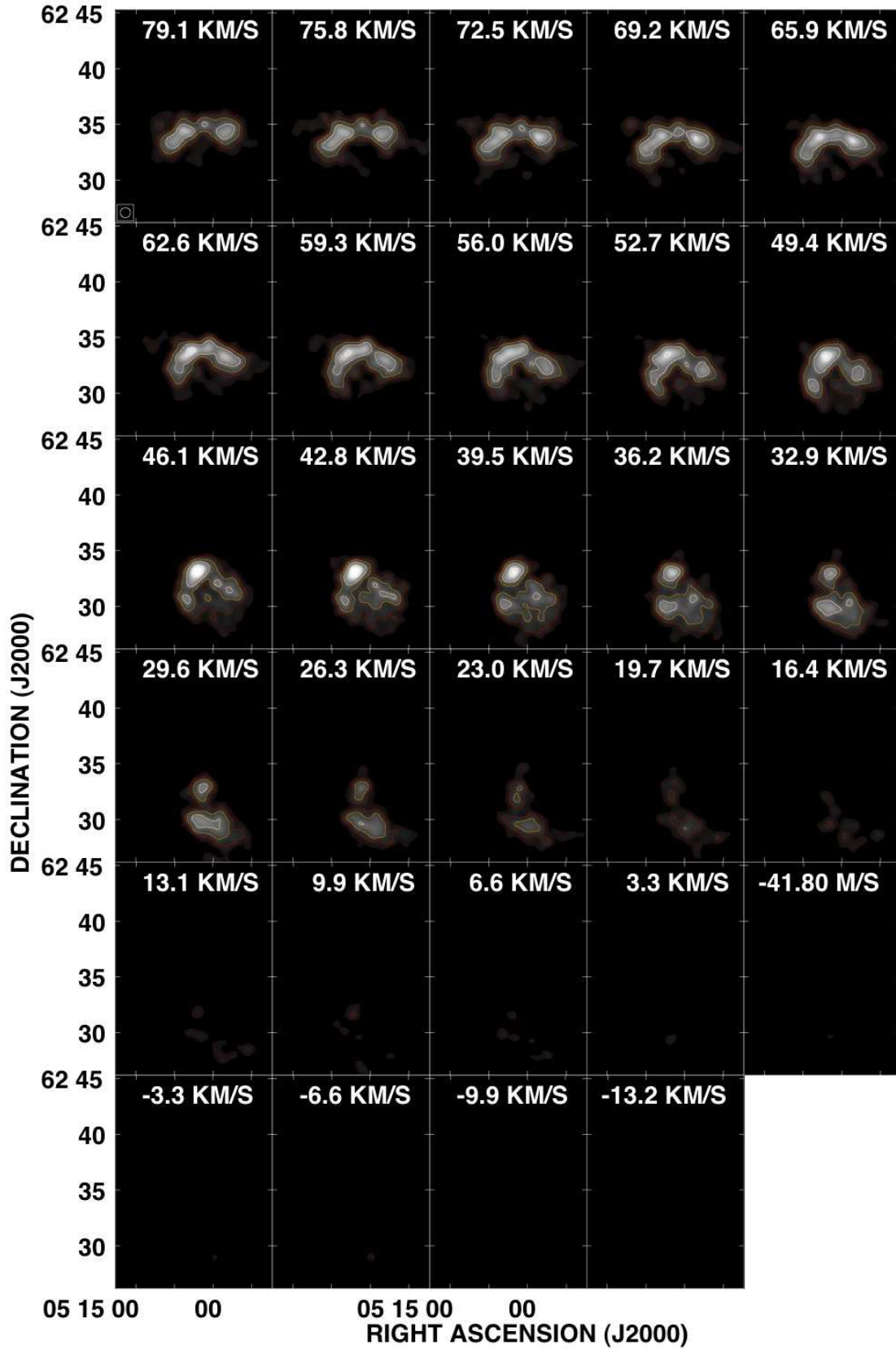


FIG. 3.— Same as Figure 2, but for the remaining 29 channels of the 54'' resolution datacube.

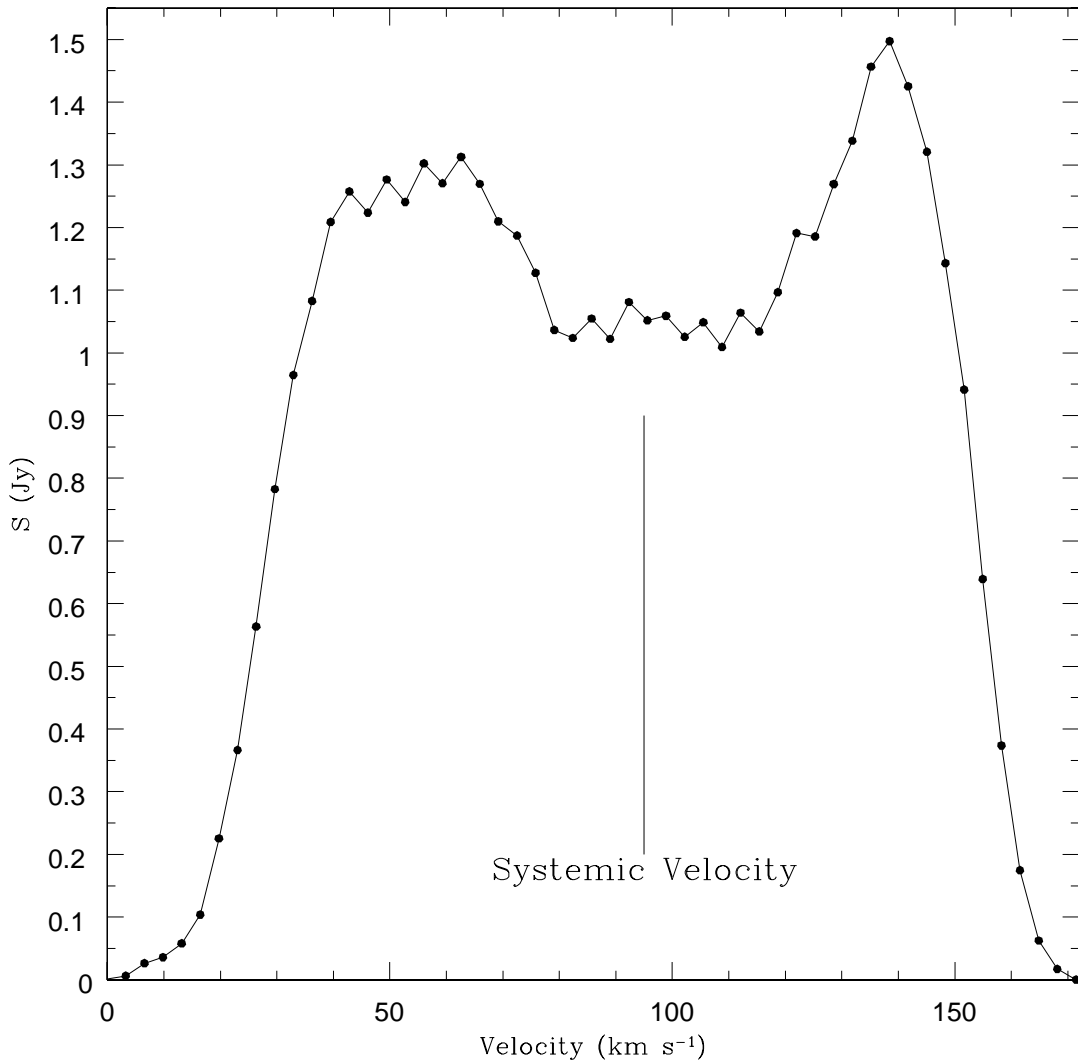


FIG. 4.— Global HI profile of UGCA 105, created by summing the flux in each channel of the 54'' resolution blanked datacube. The systemic velocity, derived from our tilted ring analyses (see Section 3.1), is $90.8 \pm 2.0 \text{ km s}^{-1}$.

ics are well-behaved and amenable to detailed rotation curve analysis (see next subsection).

The neutral gas disk (HI radius ~ 7.2 kpc at the $N_{\text{HI}} = 10^{20} \text{ cm}^{-2}$ level) is roughly twice as large as the stellar disk at the B-band R_{25} isophote (see Table 1). To allow a straightforward comparison of the stellar and gaseous disk components, we present in Figure 6(a) an optical three-color image (created from *Digitized Sky Survey* images) overlaid with contours of HI column density. The high surface brightness stellar disk is cospatial with the dense inner regions of the gaseous disk ($N_{\text{HI}} > 10^{21} \text{ cm}^{-2}$). Figure 1 verifies that most of the ongoing star formation in UGCA 105 is also concentrated within this inner disk (see further discussion below).

Figure 6(b) shows the same three color image overlaid with color-coded isovelocity contours. As expected, the high surface brightness stellar disk is located within the innermost and well-behaved section of the intensity weighted velocity field. The extent of the well-sampled velocity field compared to the stellar disk, and its coher-

ent rotation at large galactocentric radii, immediately imply that there is a substantial mass component in the outer disk regions. We explore this in more detail in the next subsections.

At the spatial resolution of these data (~ 890 pc) we can perform only bulk comparisons of the local HI surface density with regions of ongoing star formation. Such a first order comparison is shown in Figure 7, where HI column density contours at the $(10, 12.5, 15) \times 10^{20} \text{ cm}^{-2}$ levels are overlaid on zoomed versions of the same 3-color optical and continuum-subtracted $\text{H}\alpha$ images as shown in Figure 1. Most, but not all, of the ongoing star formation in UGCA 105 is coincident with the highest surface density regions of the neutral gas disk. A detailed comparative study of the local neutral gas surface density and the ongoing star formation in UGCA 105 would be very fruitful, and we defer such discussion until higher spatial resolution HI imaging is available.

3.2. Dynamical Analysis of the UGCA 105 Neutral Gas Disk

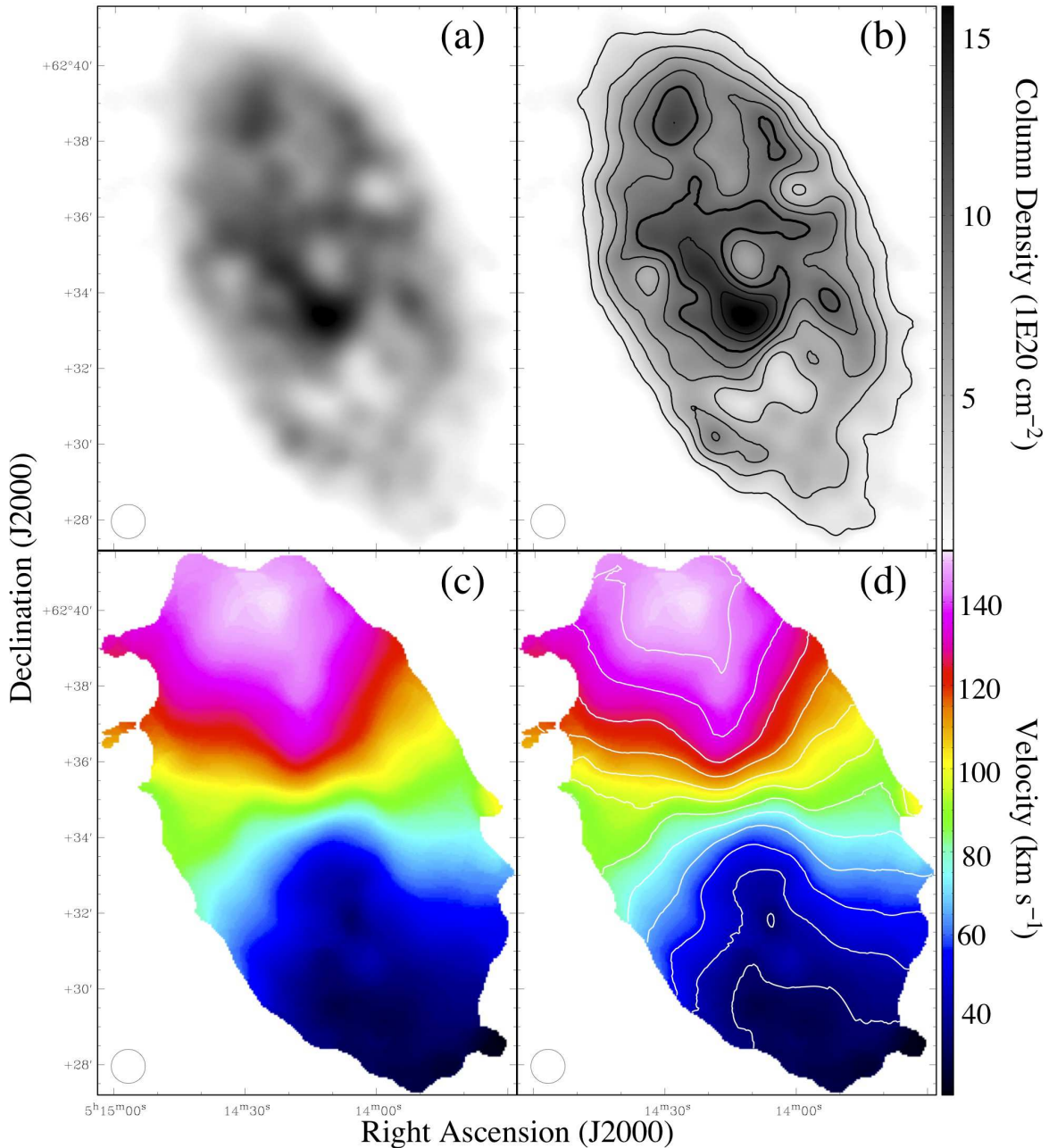


FIG. 5.— Comparison of the HI column density distribution (*a*, *b*) and the integrated velocity field (*c*, *d*); the beam size is $54''$. The contours in *b* are at the $(2, 4, 6, 8, 10, 12, 14, 16) \times 10^{21} \text{ cm}^{-2}$ level. The contours in *d* show velocities between 35 and 145 km s^{-1} , separated by 10 km s^{-1} . UGCA 105 is undergoing well-ordered rotation throughout most of the disk.

The proximity of UGCA 105, and the well-ordered rotation throughout most of the HI disk, are conducive to detailed rotation curve analysis. A first order understanding of the bulk kinematics is provided by a simple position velocity (PV) cut through the full HI cube. By varying the position angle of the PV cut, one can easily identify the direction of maximum velocity gradient in the galaxy; this offers a simple prior on the kinematic position angle. Similarly, the position angle of zero velocity gradient will be very close to the kinematic minor axis. As shown in Figure 8, the PV cut along the major axis (which is not corrected for inclination) already shows a flat rotation profile outside of the inner solid body disk. Similarly, the velocity of the kinematic minor axis is in good agreement with the systemic velocity

derived above and shows a flat profile in velocity as a function of position.

Given these first constraints on the gas kinematics, we next fitted tilted ring models to the velocity field using tools in the *GIPSY* software package³. In an iterative sequence, we fit the systemic velocity (V_{sys}), dynamical center position, position angle (P.A.), inclination (i) and rotational velocity for the galaxy as a whole, and for the receding and approaching sides individually. The priors on systemic velocity (see Figures 4 and 8) and on kinematic position angle (see Figure 8) allow one to narrow the starting points in parameter space (although checks

³ The Groningen Image Processing System (GIPSY) is distributed by the Kapteyn Astronomical Institute, Groningen, Netherlands.

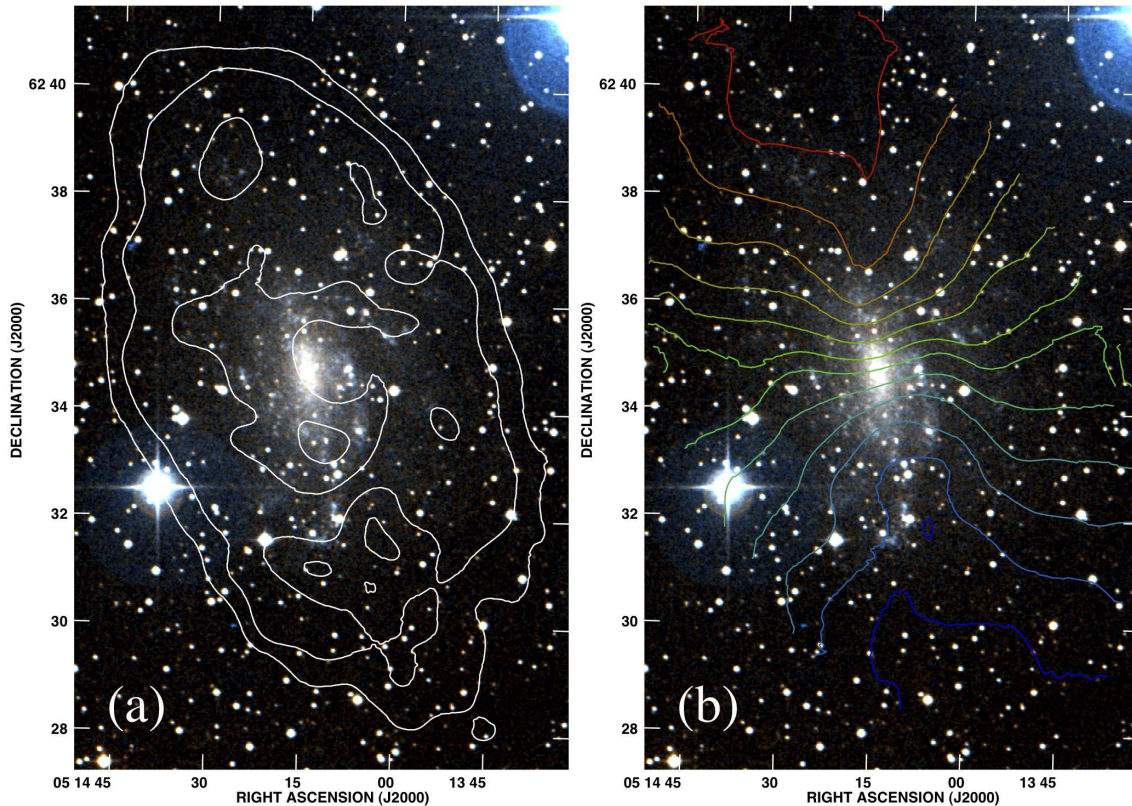


FIG. 6.— *Digitized Sky Survey* 3-color optical images, overlaid with contours showing HI column density (a) and intensity weighted velocity (b). The contours in (a) and (b) are at levels of $(2.5, 5, 10, 15) \times 10^{20} \text{ cm}^{-2}$ and $(35, 45, 55, 65, 75, 87, 95, 105, 115, 125, 135, 145) \text{ km s}^{-1}$, respectively. Most of the high surface brightness stellar disk is located within the dense inner gaseous disk ($N_{\text{HI}} > 10^{21} \text{ cm}^{-2}$).

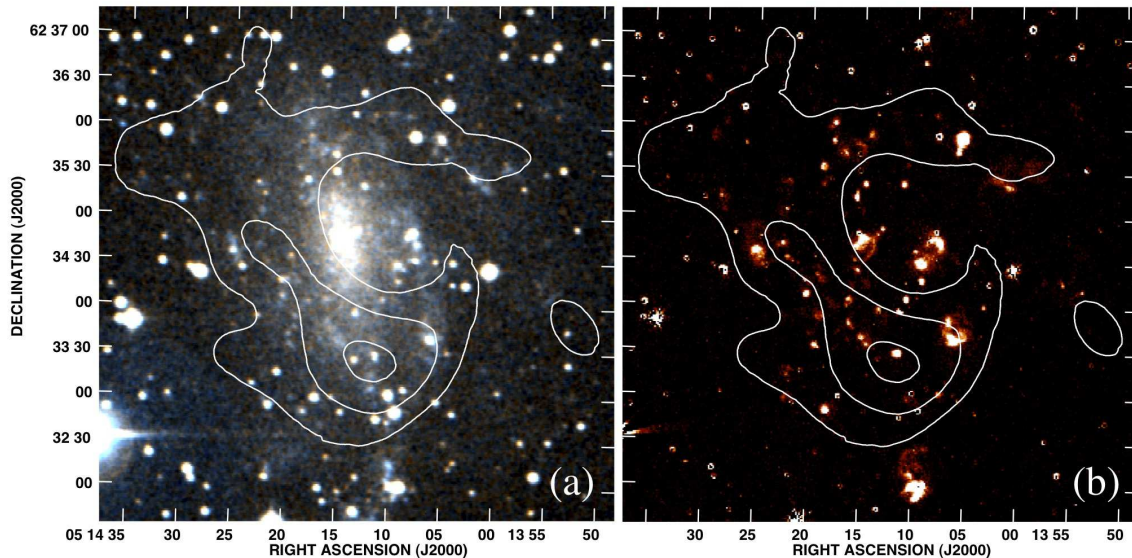


FIG. 7.— *Digitized Sky Survey* 3-color optical image (a) and continuum-subtracted $\text{H}\alpha$ image (b) of the inner disk of UGCA 105, overlaid with HI column density contours at the $(10, 12.5, 15) \times 10^{20} \text{ cm}^{-2}$ levels. Most, but not all, of the ongoing star formation in UGCA 105 is located in the regions of highest neutral gas surface density. A detailed comparative study of the neutral gas properties and the ongoing star formation requires higher spatial resolution data.

against the same procedures executed without the priors showed no difference in the final best-fit result). We experimented with all available sequences of parameter fitting (i.e., fitting each different variable in turn throughout the procedure); the final result is robust against any choice of fitting sequence.

We obtained optimal rotation curve fits to the observed low resolution velocity field by fixing parameters as follows: $i = 55^\circ \pm 2^\circ$; P.A. = $15^\circ \pm 2^\circ$ (which is in good agreement with the apparent major axis position angle of the stellar disk; see, e.g., Figure 1); $V_{\text{sys}} = (90.8 \pm 2.0) \text{ km s}^{-1}$; and dynamical center position $(\alpha, \delta, \text{J2000}) =$

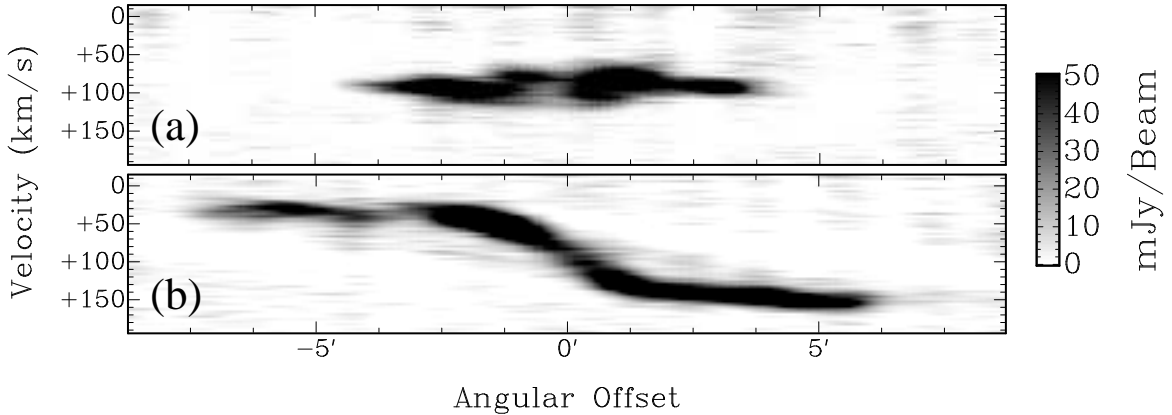


FIG. 8.— Minor (position angle 105.12° , measured east of north; *a*) and major (position angle 15.12° , measured east of north; *b*) axis position-velocity diagrams. Each cut is centered on the dynamical center of the galaxy ($5^h 14^m 13.76^s$, $62^\circ 34' 53.0''$) as derived from the rotation curve analysis (see Figure 9 and discussion in § 3.2).

($5^h 14^m 13.76^s$, $62^\circ 34' 53.0''$). The resulting curves are shown at both $27''$ and $54''$ resolution in Figure 9; note that the solid black points use annuli with $27''$ widths (i.e., half of the beam size) and are only technically independent at every other data point. In Figure 9 we also show the profiles of kinematic position angle and inclination (derived using fixed values for V_{sys} and dynamical center position); there are only minor variations of these parameters with radius. The rotation curve clearly demonstrates solid-body rotation to $\sim 100''$ (1.5 kpc), a more shallow rise between 1.5 and 5.0 kpc, and a flattening at $\sim 72 \text{ km s}^{-1}$ to the detection limit in the outer disk (~ 7.5 kpc). Assuming circular orbits, the implied dynamical mass at this outermost radius is $(9 \pm 2) \times 10^9 M_\odot$.

This dynamical mass measurement can be directly compared to the total baryonic mass of UGCA 105. As noted above, our *JVLA* images reveal a total HI mass of $(4.3 \pm 0.5) \times 10^8 M_\odot$. Given the low mass of UGCA 105, it is likely to be a metal-poor system (see, e.g., the mass-metallicity relationship presented by Tremonti et al. 2004) whose molecular content is difficult to measure observationally. While Leroy et al. (2005) do find a marginal detection of CO in UGCA 105 ($I_{\text{CO}} = (0.61 \pm 0.16) \text{ K km s}^{-1}$), a direct measurement of the molecular mass in this galaxy is not currently available. Thus, following Cannon et al. (2010), we include a 35% correction for Helium and molecular material and adopt $(5.9 \pm 0.7) \times 10^8 M_\odot$ as the total gas mass (M_{gas}) of UGCA 105.

Our tilted ring analysis also allows us to examine the radial behavior of HI mass density per unit area throughout the gas disk. We again used the *GIPSY* software package to integrate the HI flux per unit area, in concentric rings separated by the beam widths, after correcting for inclination and the galaxy’s major axis position angle (see Figure 9 and discussion above). The resulting plot, shown in Figure 10, demonstrates that the innermost few hundred pc of the HI disk contains significantly less neutral gas per unit area than the regions further out in the disk; this could be tantalizing though marginal evidence for a molecular region in the inner disk (indeed, the marginal CO detection by Leroy et al. 2005 is in close proximity to the dynamical center position). The highest mass surface densities are located between ~ 1 –2 kpc

from the dynamical center.

3.3. Luminous and Dark Mass Components in UGCA 105

The infrared luminosity of UGCA 105 is estimated using the 2MASS broadband infrared photometry presented in the 2MASS Extended Source Catalog (Jarrett et al. 2000). The total J, H, and K_S magnitudes are 12.274 ± 0.030 , 11.510 ± 0.037 , and 11.364 ± 0.052 , respectively. We assume a negligible difference between K and K_S magnitudes and adopt $L_{K, \odot} = +3.33$ (Cox 2000; Bessell 1979). The total K-band luminosity of UGCA 105 is found to be $L_K = \sim 7.8 \times 10^7 L_\odot$ after correcting for Milky Way extinction.

To derive the mass of the stellar component, we apply the techniques discussed in detail in Cannon et al. (2010). Briefly, we use the models presented in Bell & de Jong (2001), which take as input the observed color and luminosity of a stellar population. The models allow one to estimate a stellar mass-to-light ratio (M/L) assuming a range of metallicities, initial mass functions, and galaxy evolution properties. Given the substantial Milky Way foreground screen, the near-infrared colors are optimal; further, these colors are less affected by recent or ongoing star formation within UGCA 105 than are optical colors. Applying the model M/L ratios and the observed K-band luminosity, we can then estimate the stellar mass of UGCA 105. Using this approach we find that the underlying stellar mass in UGCA 105 is $M_* = (1.8 \pm 0.8) \times 10^8 M_\odot$.

The sum of the luminous baryons (gas and stars) in UGCA 105 is estimated to be $M_{\text{bary}} \simeq 8 \times 10^8 M_\odot$. At the last measured point of the HI rotation curve (see Figure 9), the implied interior dynamical mass is $\sim 9 \times 10^9 M_\odot$. While we are sensitive to neither the molecular component of the ISM nor to the cool dust component with the present observations, recent investigations have shown that these components are not substantial mass reservoirs in the interstellar media of low-mass galaxies (see, e.g., Leroy et al. 2005, Walter et al. 2007, Schrubba et al. 2012, and various references therein). We conclude that UGCA 105 is a typical dwarf galaxy whose mass is dominated by dark matter (especially at large galactocentric radii). These results are similar to those found in recent studies of other nearby dwarf galaxies (see, e.g.,

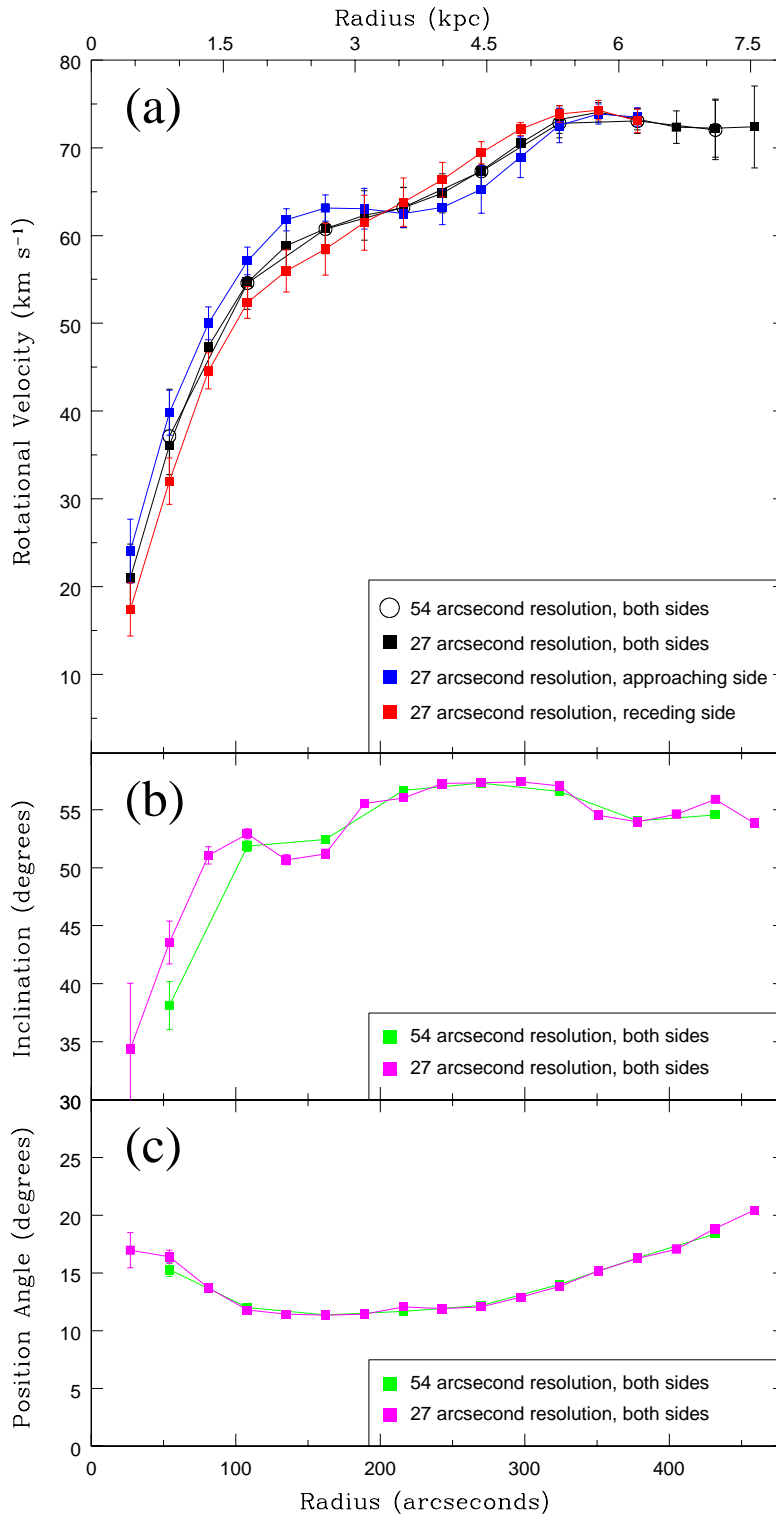


FIG. 9.— (a) Rotation curves of UGCA 105 derived by fitting tilted ring models to the intensity-weighted velocity field. The open circles use annuli separated by the full beam width ($54''$) and are independent at each measured position. The solid black points use annuli with $27''$ widths (i.e., half of the beam size) and are only technically independent at every other data point. The black points are fit to both sides of the disk simultaneously. The blue and red curves fit tilted rings to either the approaching (blue) or receding (red) sides of the disk, using the same parameters of V_{sys} (90.8 km s^{-1}), inclination (54.9°), dynamical center position ($5^{\text{h}}14^{\text{m}}13.76^{\text{s}}$, $62^\circ34'53.0''$), and position angle (15.12°) as used for the $27''$ resolution fit to both sides of the disk. The lower panels show the inclination angle (b) and the kinematic major axis position angle (c) as functions of radius. The profiles shown in (b) and (c) were derived using fixed values for V_{sys} and dynamical center position; there are only minor variations of these parameters with radius.

the detailed discussion in Oh et al. 2008, Cannon et al. 2010, and Oh et al. 2011).

4. CONCLUSIONS

We have presented new low resolution *JVLA* imaging of the nearby low mass galaxy UGCA 105. This system

has remained comparatively under-studied in the astrophysical literature. The system is actively forming stars (as traced by high surface brightness $\text{H}\alpha$ emission; see Kennicutt et al. 2008) and is located in sufficient proximity ($3.39 \pm 0.25 \text{ Mpc}$; Jacobs et al. 2009, Tully et al. 2009) to allow detailed dynamical analysis. In this work we

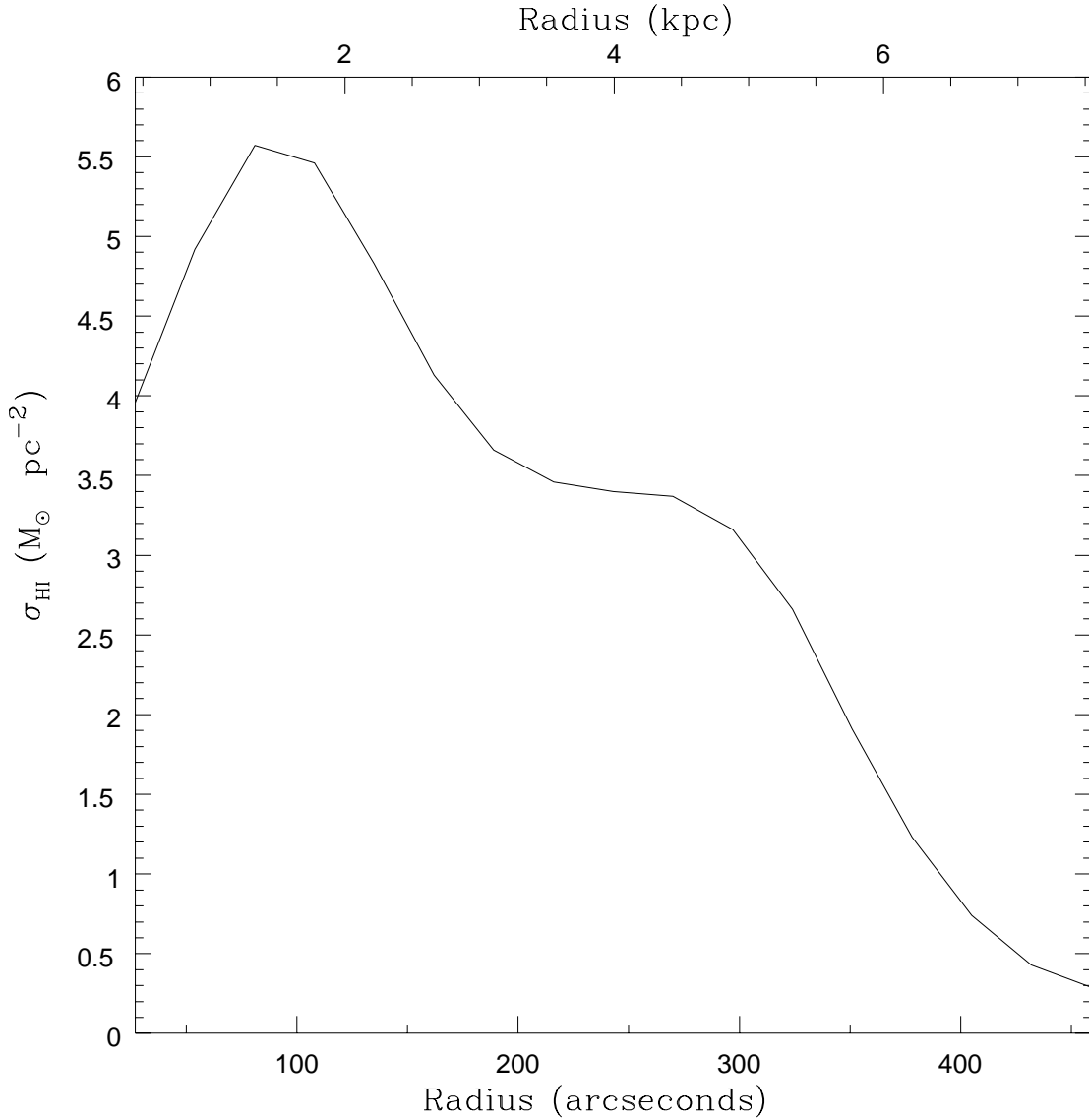


FIG. 10.— Radially averaged HI mass surface density profile of UGCA 105, created by summing HI emission in concentric rings emanating from the dynamical center found in our rotation curve analysis. The solid line was created using annuli spaced by $27''$ (half of the $54''$ circular beam size; see discussion in § 3.2 and Figure 9).

present the first spatially resolved study of the neutral gas dynamics of UGCA 105.

At $54''$ (890 pc) resolution, the neutral gas morphology and kinematics are measured with high fidelity with these new *JVLA* data. The HI gas spans $\sim 175 \text{ km s}^{-1}$; sampled over ~ 54 channels each separated by 3.3 km s^{-1} , the system displays a classical “butterfly diagram” and double-horned integrated line profile. We recover 98% of the single dish flux (Springob et al. 2005), with no correction for HI self absorption applied. We derive a systemic velocity of $90.8 \pm 2.0 \text{ km s}^{-1}$; UGCA 105 has an unusual velocity given its location well outside the Local Group.

The integrated HI column density distribution of UGCA 105 contains high surface density gas ($N_{\text{HI}} > 10^{21} \text{ cm}^{-2}$) throughout the extent of the luminous stellar disk. While we see evidence for regions of low column density (i.e., HI holes or shells) and also evidence for spatial agreement between regions of ongoing star formation (as traced by $\text{H}\alpha$ emission) and high column density gas, we defer a detailed treatment until higher spatial resolution

HI imaging is available. We do note that the inclination corrected surface mass density profile of UGCA 105 falls in the regions closest to the dynamical center; this could be interpreted as marginal evidence for a molecular region in the inner disk.

These new *JVLA* data offer an opportunity to study the bulk neutral gas dynamics of UGCA 105. The system displays well-ordered rotation throughout the neutral gas disk and the intensity weighted isovelocity contours are parallel throughout the entire inner disk (cospatial with the high surface brightness stellar disk). We use standard GIPSY tilted ring analysis in order to fit the observed velocity field of UGCA 105. Regardless of how the parameters are fixed, we find a robust and well constrained rotation curve at all galactocentric radii. The profile rises steeply in the innermost $\sim 1.5 \text{ kpc}$, rises more slowly in the region from $\sim 1.5 \text{ kpc}$ to $\sim 5 \text{ kpc}$, and then remains flat at 72 km s^{-1} out to the last measured point (7.5 kpc). The total dynamical mass of UGCA 105, derived from this rotation curve, is $M_{\text{dyn}} = (9 \pm 2) \times 10^9 M_{\odot}$.

This dynamical mass is larger than the sum of the luminous components [$M_{\text{gas}} = (5.9 \pm 0.7) \times 10^8$ inclusive of a 35% correction for Helium and molecular material; $M_{\star} = (1.8 \pm 0.8) \times 10^8 M_{\odot}$] by a factor of ~ 10 ; UGCA 105 is a typical, dark matter dominated dwarf galaxy (see, e.g., Oh et al. 2008, Oh et al. 2011, and references therein).

The proximity and favorable inclination (55°) of UGCA 105 make it a promising target for high resolution studies of both star formation and rotational dynamics in a nearby low-mass galaxy. In particular, B configuration *JVLA* observations would achieve a synthesized physical resolution element of order 100 pc; the high HI surface brightness would guarantee high signal to noise measurements at this spatial resolution. The resulting datasets would facilitate detailed analyses of the interplay of neutral gas and recent star formation on ~ 100 pc scales.

The authors would like to thank the National Radio Astronomy Observatory for making the ‘‘Observing for University Classes’’ program available to the astronomical community, and for organizing a very enjoyable and productive visit to the Science Operations Center in Socorro, New Mexico. We acknowledge a helpful anonymous referee whose suggestions helped to improve the quality of this manuscript. J.M.C. would like to acknowledge useful discussions with Bradley Jacobs, Igor Karachentsev, Robert C. Kennicutt, Jr., and Janice Lee. J.M.C. would like to thank Paul Overvoorde, Daniel Hornbach, Kathleen Murray, Ann Minnick, and Tonnis ter Veldhuis, whose contributions to this project allowed it to be a success. Finally, the authors would like to thank Macalester College for generous research and teaching support.

REFERENCES

- Bell, E. F., & de Jong, R. S. 2001, *ApJ*, 550, 21
 Bessell, M. S. 1979, *PASP*, 91, 589
 Cannon, J. M., Salzer, J. J., & Rosenberg, J. L. 2009, *ApJ*, 696, 2104
 Cannon, J. M., Haynes, K., Most, H., et al. 2010, *AJ*, 139, 2170
 Cannon, J. M., Most, H. P., Skillman, E. D., et al. 2011, *ApJ*, 735, 35
 Caplan, J., & Deharveng, L. 1986, *A&A*, 155, 297
 Condon, J. J., Cotton, W. D., Greisen, E. W., et al. 1998, *AJ*, 115, 1693
 Cox, A. N. 2000, *Allen’s Astrophysical Quantities* (4th ed.; New York; Springer)
 de Vaucouleurs, G., de Vaucouleurs, A., Corwin, H. G., Jr., et al. 1991, Volume 1-3, XII, 2069 pp. 7 figs.. Springer-Verlag Berlin Heidelberg New York
 Jacobs, B. A., Rizzi, L., Tully, R. B., et al. 2009, *AJ*, 138, 332
 Jarrett, T. H., Chester, T., Cutri, R., et al. 2000, *AJ*, 119, 2498
 Karachentsev, I. D., Sharina, M. E., Makarov, D. I., et al. 2002, *A&A*, 389, 812
 Karachentsev, I., Drozdovsky, I., Kajsins, S., et al. 1997, *A&AS*, 124, 559
 Karachentsev, I. D., & Kaisin, S. S. 2010, *AJ*, 140, 1241
 Kennicutt, R. C., Jr., Lee, J. C., Funes, S. J., Jose G., Sakai, S., & Akiyama, S. 2008, *ApJS*, 178, 247
 Lee, J. C., Gil de Paz, A., Tremonti, C., et al. 2009, *ApJ*, 706, 599
 Leroy, A., Bolatto, A. D., Simon, J. D., & Blitz, L. 2005, *ApJ*, 625, 763
 Mateo, M. L. 1998, *ARA&A*, 36, 435
 Oh, S.-H., de Blok, W. J. G., Walter, F., Brinks, E., & Kennicutt, R. C., Jr. 2008, *AJ*, 136, 2761
 Oh, S.-H., de Blok, W. J. G., Brinks, E., Walter, F., & Kennicutt, R. C., Jr. 2011, *AJ*, 141, 193
 Rizzi, L., Tully, R. B., Makarov, D., et al. 2007, *ApJ*, 661, 815
 Schlegel, D. J., Finkbeiner, D. P., & Davis, M. 1998, *ApJ*, 500, 525
 Schrubba, A., Leroy, A. K., Walter, F., et al. 2012, *AJ*, 2012, 143, 138
 Springob, C. M., Haynes, M. P., Giovanelli, R., & Kent, B. R. 2005, *ApJS*, 160, 149
 Tikhonov, N. A., Karachentsev, I. D., Bilkina, B. I., & Sharina, M. E. 1992, *Astronomical and Astrophysical Transactions*, 1, 269
 Tremonti, C. A., Heckman, T. M., Kauffmann, G., et al. 2004, *ApJ*, 613, 898
 Tully, R. B., Rizzi, L., Shaya, E. J., et al. 2009, *AJ*, 138, 323
 Walter, F., Cannon, J. M., Roussel, H., et al. 2007, *ApJ*, 661, 102